

TREATMENT PLANNING ALGORITHMS PART 1 OF 2

Dr Simon Thomas¹ [Head of Medical Physics and Clinical Engineering at Addenbrooke's Hospital, Cambridge University Hospitals NHS Trust, UK] gives an introduction to the main types of photon algorithms used in treatment planning systems

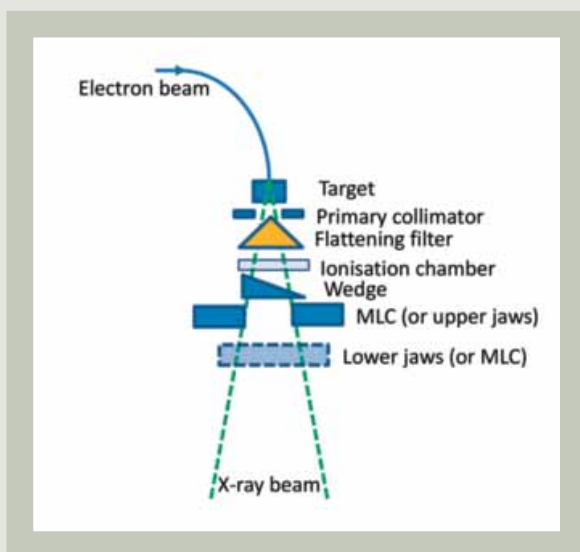


FIGURE 1. Schematic of typical linac head (not to scale)

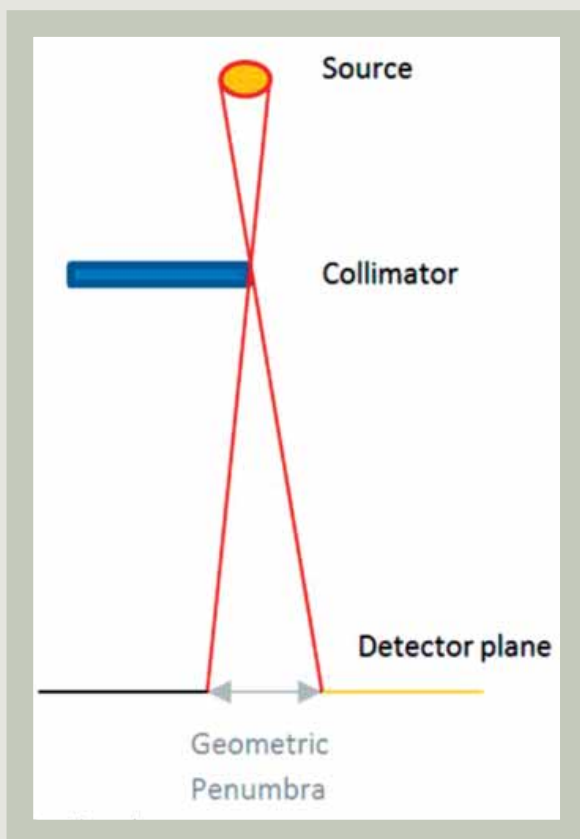


FIGURE 2. Geometric penumbra

Introduction

The aim of this tutorial is to give users of treatment planning systems an understanding of the algorithms they are using. It will cover the algorithms currently in common use in treatment planning systems in the UK and will include:

- dose calculation for megavoltage photons;
- inverse planning and optimisation, and
- dose calculation for charged particles.

I will cover the generalities of each algorithm, but not the precise implementation by individual manufacturers.

Dose deposition in tissue is dominated by charged particle (electron) transport, from electrons released in Compton and other interactions. In a medium that is much less dense than water, such as lung, an electron travels much further before losing its energy. This means that the beam penumbra, measured in a lung phantom, is wider than the penumbra of the same beam measured in a water phantom.

The world of treatment planning algorithms can be divided into two, known as 'type b' and 'type a',¹ based on whether or not the algorithm knows about this basic bit of physics; 'type b' algorithms are the ones that correctly model the penumbral change with density, whilst 'type a' algorithms are the ones that do not.

Several commercial systems offer a choice of algorithms, both of 'type b' (more accurate but potentially slow) and of 'type a' (less accurate but faster). Before covering the properties of linacs that need to be modelled.

Properties of linacs than need to be modelled

Multiple sources of radiation

The main source of radiation is the point in the metal target onto which the electron beam is focussed. This point is referred to as the 'focal spot', 'focus' or 'primary source'.

The shape of the field at the patient is determined by the collimators, consisting of the jaws and the multileaf collimator (MLC). The MLC position varies between manufacturers. For Elekta, the MLC replaces the upper jaws, as shown in figure 1. Siemens uses the MLC to replace the lower jaws, whilst Varian keeps both sets of jaws and has the MLC below the lower jaws.

In machines with a flattening filter, the scattered radiation from the filter acts as the second largest source of radiation. The primary collimator also acts as a radiation source. Since these components are close together in the head, these can sometimes be regarded as a single extended source. Other structures in the head of the machine (wedge, jaws, MLC) all scatter radiation and contribute, to a lesser extent, to the radiation coming from the head.

The fact that radiation comes from multiple sources influences the shape of the penumbra; as shown in figure 2, the width and position of a source relative to the collimator determines the geometric penumbra.

MLC properties

The positions of the MLCs and jaws need to be known by most algorithms (with the possible exception of measured beam models) to model the geometric penumbra.

The shape of the collimating edge also influences the shape of the penumbra. This will differ between the jaws, the MLC ends and the MLC sides. The sides of the MLC have steps to minimise leakage of radiation, known as the 'tongue and groove', as shown

in figure 3. A consequence of these steps is that beam edges (defined by the position of the 50 per cent) of two nominally adjacent segments will not align to the same edge. Planning systems will vary as to how well they model this.

Photon interactions

A photon travels in a straight line until it interacts with matter. For a megavoltage photon in tissue or water, the most likely interaction is Compton scattering. The other two major interactions are the photoelectric effect (PE) and pair production (PP). All three of these interactions involve transfer of energy to a secondary electron, which then deposits energy by ionisation as it travels up to its maximum range. In Compton and PE, there is also energy given to a secondary or tertiary photon, which will travel a greater distance before possibly interacting to deliver dose at a distance from the first interaction. In PP, the positron deposits dose by ionisation in a similar manner to the electron, before annihilating with an electron to produce two photons of 511 keV, which will contribute to the dose at a distance from the first interaction.

Hence, a photon interaction leads to dose being deposited over a range of distances and directions, most locally (within the range of the electrons produced) and some at a greater distance (due to secondary photons).

Converting HU to density

The Hounsfield unit (HU) of a CT scanner is generally defined as:

$$HU = 1000 \times \frac{(\mu - \mu_w)}{\mu_w}$$

where μ is the attenuation coefficient of x-rays at the point of interest, and μ_w is the attenuation coefficient of water. For the kV x-rays usually used in CT scanners, the Compton effect dominates in low-Z materials such as lung, fat and muscle, but a substantial proportion of the attenuation is PE in higher Z materials such as bone. In the Compton region, μ is almost completely proportional to ρ_e , the electron density relative to water, giving rise to the solid line in figure 4. For bone-like materials, the presence of calcium leads to the dashed line in figure 4.

The slope of the solid line does not

vary with energy; however, the slope of the dashed line varies between scanners and between different kV settings on the same scanner.

For the density correction methods generally used with 'type a' algorithms, the density is required as a means of correcting the attenuation in tissue relative to that in water. Since for the MV x-rays used in radiotherapy the dominant attenuation process is Compton scatter (even in bone), conversion using figure 4 (or a similar curve measured for your own scanner with a phantom with inserts of known electron density) is all that is required. A decision has to be made as to where one jumps from the solid blue line to the dashed red line. Is a pixel with an HU of 150 a piece of dense low-Z material (in which case $\rho_e = 1.15$), or very low density bone (in which case $\rho_e = 1.08$)? In practice there are very few biological materials with HU between 100 and 260, so pragmatically a decision can be made to use the solid blue line below 100 HU and the dashed red line above 100 HU. However, some phantom materials (especially Perspex with $\rho_e = 1.16$) can give problems; this is why it is sometimes necessary for a planning system to have different HU to density tables for phantoms and patients.

Most of the 'type b' algorithms also require the physical density ($g\ cm^{-3}$). This is harder to determine directly from the CT. One approach is to measure a curve similar to figure 4, with a phantom with inserts of known physical density. However, care needs to be taken to ensure that the elemental composition of your inserts mimics patient materials. If it does not, you will have no better results than if you had assumed that all materials are effectively 'dense water'. Stoichiometric methods, which start by assuming the elemental compositions of different tissues, can be used to get a more accurate conversion curve.

Some planning systems (e.g. Pinnacle, TomoTherapy) use an HU to physical density curve as their only HU calibration curve. Tables of physical density to attenuation coefficients are used to get back to the answers they would have got if they had used electron density in the first place.

Monte Carlo

Anything that picks events from a probability distribution using random numbers is a Monte Carlo simulation. In

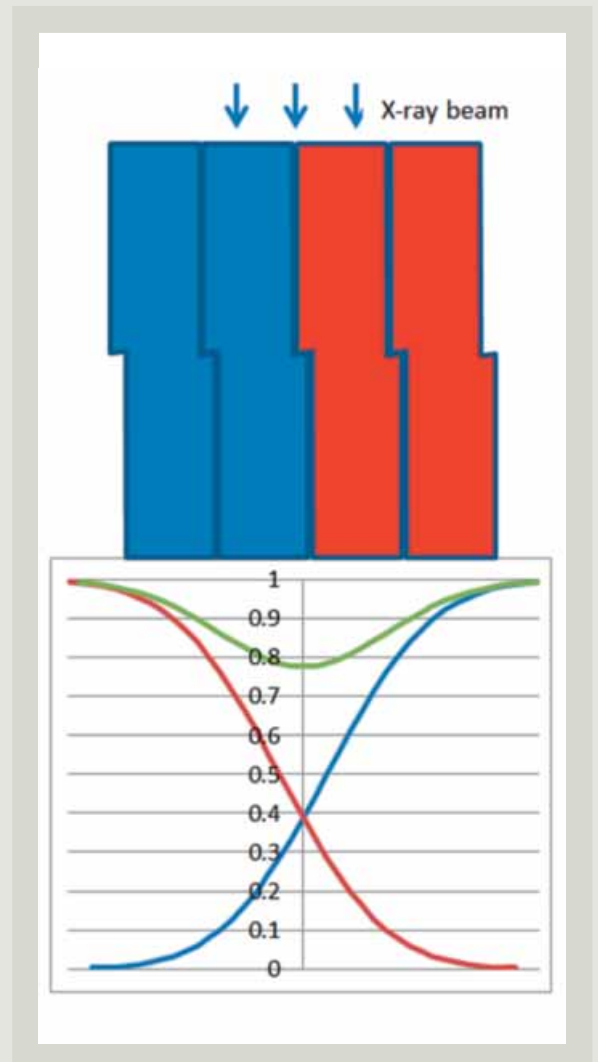


FIGURE 3. Tongue and groove effect. The blue and red profiles correspond to the profile when MLC leaves of the same colour are closed. The green line is the summation of the dose from two adjacent segments

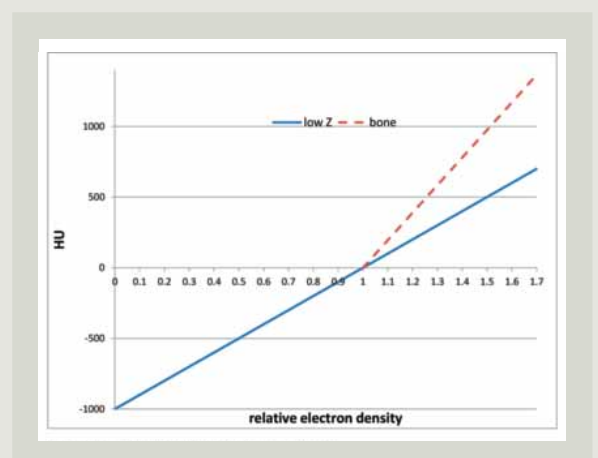


FIGURE 4. The relationship between HU and electron density

→ AFFILIATION

Head of Medical Physics and Clinical Engineering at Addenbrooke's Hospital, Cambridge University Hospitals NHS Trust, UK

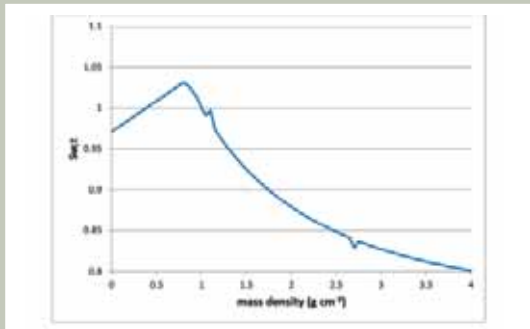


FIGURE 5. Stopping power ratio as a function of density

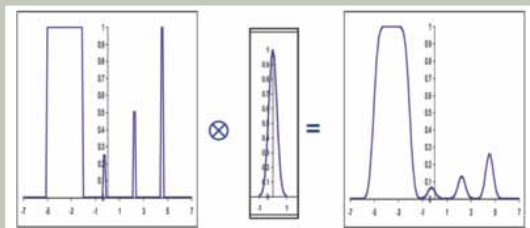


FIGURE 6. A 1D convolution

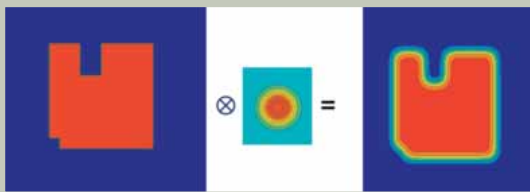


FIGURE 7. A 2D convolution

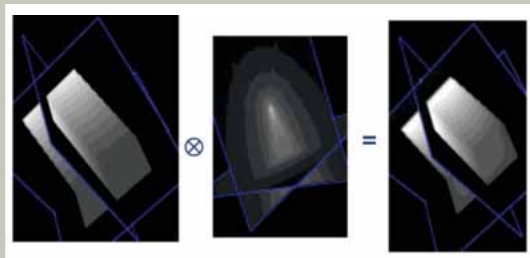


FIGURE 8. A 3D convolution

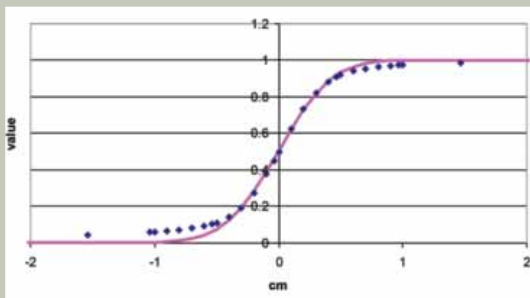


FIGURE 9. An error function (solid line) fitted to a measured beam profile (points)

the context of this tutorial, we will restrict this to following the interactions of photons and electrons. In principle, this can be done by knowing the cross sections of all the interaction processes (PE, Compton, PP etc.) for a continuum of energies in a particular material. The cross section data should also include information regarding the angular distributions of scattered particles.

Using random numbers and knowledge of the probability of interactions occurring, one can randomly select the distance a particle travels to the next interaction, as well as the type of interaction the particle experiences. The primary photons generate secondary photons and electrons, which themselves undergo the same process (including the generation of tertiary particles and so on) until all the energy is absorbed. The process is then repeated for a large enough number of primary particles (histories) such that the result has an acceptable level of statistical uncertainty.

However, electrons have large cross sections, making their mean free path much shorter than photons. As a result, far too many calculations are needed to model electron paths; approximations are used to make calculations manageable. Different MC codes make different assumptions to increase speed. These approximations mean that we are no longer being true to the laws of physics. All algorithms end up making some trade-offs between speed and accuracy.

MC calculations are subject to statistical uncertainty in dose, proportional to $1/\sqrt{N}$, where N is the number of histories. As a result, calculations need large numbers of histories (in the order of 10^4 per voxel to get down to an uncertainty of 1 per cent).

The process of calculating the dose, from linac to patient, is as follows:

1. Start with an electron exiting from waveguide.
2. Follow it and its descendants through targets, primary collimators, ion chambers etc.
3. Track it through patient-dependent structures (jaws, MLC etc.).
4. Track it through the patient (as modelled from CT data set).

MC planning systems can speed up the process by precalculating to the

end of step 2 and storing a phase-space file. Several commercial systems (e.g. Monaco, BrainLab and RayStation) use code based on the Voxel Monte Carlo (VMC)^{2,3} code and code derived from it, such as XVCM and VMC++. Eclipse uses Macro Monte Carlo (MMC)⁴ for electron calculations. These codes give much faster calculations than general purpose Monte Carlo codes, at the price of introducing a number of simplifying approximations.

Where a general MC code such as EGS4 or EGSnrc⁵ is designed to describe electron transport in a wide range of energies and materials, for arbitrary geometries, VMC restricts itself to electrons with a kinetic energy of 1 to 30 MeV, and to low-Z materials with densities of 0 to 3 kg m⁻³, and only performs dose calculations in rectangular geometries (as defined by the patient CT image). VMC also uses a simplified version of the distribution for multiple scattering, and uses energy cut-offs (typically 500 keV for electrons and 50 keV for photons) to increase speed. MMC speeds calculations by transporting electrons in large-scale macroscopic steps through the absorber.

Most of the convolution/superposition algorithms (described later) use Monte Carlo calculations to generate the kernels which describe how the dose from a single photon interaction is deposited in water.

Dose to water or dose to tissue

For Monte Carlo algorithms and some other 'type b' algorithms, a distinction is made between 'dose to water' D_{med}^w and 'dose to tissue' D_{med}^t . The subscript 'med' in both cases indicates that the attenuation and scattering in the medium is accounted for. 'Dose to tissue' is the default result of a Monte Carlo calculation that takes the energy deposited in a small volume of tissue and divides it by the mass of tissue in the small volume to give the dose. 'Dose to water' is the dose that would have been received by a small volume of water located at the same point.

Conversion from 'dose to tissue' to 'dose to water' requires the application of Bragg-Gray cavity theory, which leads to the equation:

$$D_{med}^w = D_{med}^t S^{w,t} \text{ where } S^{w,t} \text{ is the water to tissue ratio of mass}$$

collision stopping power, averaged over the energy spectrum. $S^{w,f}$ varies with the density and elemental composition of the tissue, and planning systems will differ on how they calculate this. For example, Monaco has a set of 11 equations that attempt to fit $S^{w,f}$ as a function of density and energy. Typical values of $S^{w,f}$ (for a spectrum of mean energy 2 MeV as a function of density) are shown in figure 5.

For most tissues other than bone, the value is within a few percent of unity. However, for doses inside very dense bones, the two doses differ by up to 20 per cent.

There is still considerable debate about whether to report dose to water or dose to tissue.⁶ The argument in favour of dose to water is that reference dosimetry of linacs is based on codes of practice that yield dose to water. The argument for dose to tissue is that since this is the quantity inherently computed by the planning system, the use of $S^{w,f}$ adds additional uncertainty, of a level that is possibly greater than the correction to be made in the first place. The discontinuities in figure 5 at densities of 1.1 and 2.7 are examples of these uncertainties. A curve that is a function of mass density cannot distinguish between two materials (e.g. ICRU 'bone' and ICRP 'bone') with the same density but very different elemental composition.

Convolution and superposition algorithms

Before covering the details of the algorithms, I will quickly revise the mathematics of convolution.

Convolution

In one dimension, the mathematical definition of convolution is:

$$[f \otimes g](x) = \int_{-\infty}^{\infty} f(x')g(x-x')dx'$$

In discrete form, as used in computer calculations, this becomes:

$$[f \otimes g](m) = \sum_n f(n)g(m-n)$$

Figure 6 demonstrates 1D convolution. The first graph represents some function f , comprising a 'top hat' function and three spikes of different sizes. The second graph contains a function g , which we will refer to as the 'kernel'. The result of convolving them

is shown in the third graph. At the position of each of the three spikes, one gets a copy of the kernel, of a size proportional to the size of the spike. The 'top hat' has its edges blurred, with the width of the blurred edge depending on the width of the kernel. An appropriate method of normalisation will be needed if the area under the kernel is not unity.

In 2D, convolution becomes:

$$[f \otimes g](x, y) = \iint_{-\infty}^{\infty} f(x', y')g(x-x', y-y')dx'dy'$$

(The reader can supply the corresponding discrete form.)

Figure 7 gives an example of a 2D convolution.

In 3D, convolution becomes:

$$[f \otimes g](x, y, z) = \iiint_{-\infty}^{\infty} f(x', y', z')g(x-x', y-y', z-z')dx'dy'dz'$$

which is illustrated in figure 8.

Figures 7 and 8 may suggest examples in radiotherapy dose calculations; we will return to these later.

A particularly interesting 1D example is the convolution of a step function (stepping from zero to unity at $x=0$) and a Gaussian (bell curve):

$$\text{Gaussian}(x) = \frac{1}{\sigma\sqrt{2\pi}} e^{-\frac{(x-\mu)^2}{2\sigma^2}}$$

When a step function and a Gaussian are convolved, the result is a function known as an 'error function', $erf(x)$:

$$\text{Gaussian} \otimes \text{step} = \frac{1}{2} \left(1 + erf\left(\frac{x-\mu}{\sigma\sqrt{2}}\right) \right)$$

Figure 9 shows the shape of an error function (pink line) plotted for $\sigma = 0.34$ cm.

The distance from the 0.2 to 0.8 value of an error function is 1.68σ . The value of σ in figure 9 was chosen to match the 20–80 per cent dose distribution for a measured beam (6 MV x-rays, 5 cm deep), shown as the blue points in the same figure. It is clear that although there is some similarity between the points and the line, agreement is not good; an error function is only a poor approximation to a beam edge profile. Radiation comes from more than one source; there is transmission through collimators and long-range scatter.

Figure 10, which shows improved agreement, was calculated by adding together an erf with a sigma of 0.3 cm, together with a 10 per cent weighted erf with a sigma of 1.0 cm, plus a

constant of 3 per cent. The resulting sum (normalised back to 1.0) gives one much closer agreement with measured data. These numbers are the result of curve fitting to the measured data, rather than from any fundamental principles. This reflects the situation in many planning systems where the beam modelling process involves playing with parameters until a good fit is found.

The size of the Gaussian from each source depends not only on the geometrical penumbra from the source but also on radiation transport in the patient or phantom. The secondary electrons released in Compton and other interactions travel some distance whilst depositing their energy; the lateral component of the electron range serves to widen the penumbra. The σ from each source is made up of a geometrical penumbra σ_{geom} combined in quadrature with a radiation penumbra σ_{radn} :

$$\sigma = \sqrt{\sigma_{geom}^2 + \sigma_{radn}^2}$$

The geometrical penumbra is independent of the density of the phantom. However, the radiation penumbra varies inversely with density (or more strictly with relative electron density), since at lower densities the electrons travel further.

Typical values might be $\sigma_{geom} = 0.26$ cm, $\sigma_{radn} = 0.15$ cm, combining to give 0.3 cm in water.

In lung of relative density 0.3, $\sigma_{radn} = 0.15/0.3 = 0.5$ cm. This combines in quadrature with σ_{geom} to give $\sigma = 0.56$ cm.

Hence, the overall penumbra in lung is about twice as wide as it is in water. The 'type b' algorithms correctly model this, whilst the 'type a' algorithms assume that σ_{radn} is not changed by changes in density.

Point kernel methods

Since the average energy required to produce an ion pair is approximately 35 eV, and the energy transferred to an electron in a photon interaction will be of the order of MeV, it will be seen that there are tens of thousands of electron interactions to each photon interaction. Practically all of the dose that is deposited is from ionisation by electrons. When considering the dose deposited per photon interaction in the primary beam, it is also ➤

➔ **FEEDBACK**
Scope welcomes your feedback!
@IPEMScope

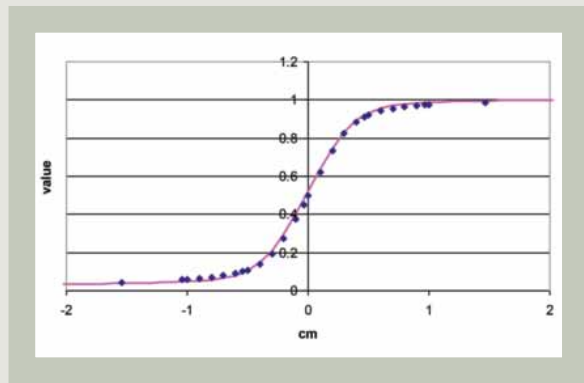


FIGURE 10. The points are as in figure 9. The line is the sum of two error functions and a constant

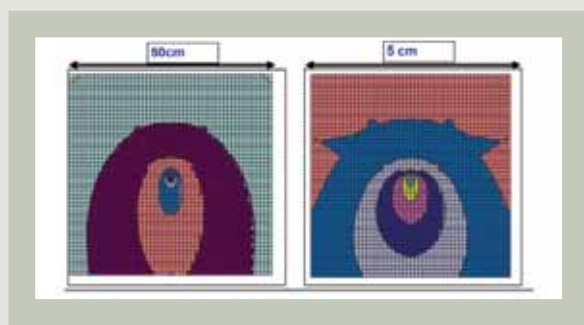


FIGURE 11. The kernel from equation 1. Note the scales of the two parts of the figure; the second part is a magnification of the centre of the first

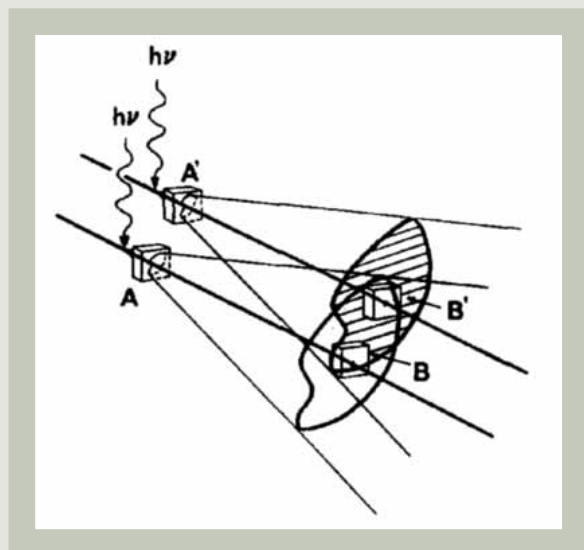


FIGURE 12. Collapsed cone from Ahjesjo⁷

necessary to consider the long-range dose deposition from secondary photons (which will themselves transfer energy to electrons when they interact with matter).

Unlike in dosimetry, where KERMA (kinetic energy released per unit mass) is used, in treatment planning algorithms it is more common to use TERMA (total energy released per unit mass). KERMA considers the energy transferred to electrons, and excludes the energy given to secondary photons. TERMA includes all the energy removed from the primary beam.

The calculation of TERMA in a patient requires the following:

- The attenuation coefficient μ for each point in the patient. This will depend on:
 - the energy spectrum of the radiation,
 - the electron density at each point (which can be calculated from the CT values).
- Strictly, the physical density is also required (since TERMA is proportional to μ/ρ). Some vendors assume that tissue is scaled water.
- Geometrical penumbra; this is accounted for by convolving with one or more Gaussians.

In a real heterogeneous patient, the TERMA calculation requires the algorithm to integrate the electron density to give the radiological path length to the calculation point.

'Point kernels' derived from Monte Carlo calculations describe how the dose from a single photon interaction is deposited in water. Some vendors fit analytical functions to the Monte Carlo derived data, such as the function described by Ahjesjo:⁷

$$h_{\nu}(r, \theta) = (A_{\nu} e^{-a r} + B_{\nu} e^{-b r}) / r^2 \quad (1)$$

where A , a , B and b are functions of angle, tabulated for a number of energies. The first term relates mainly to primary dose (short range), the second mainly to scattered photons (long range). Some systems implement these as two separate convolutions using two different grid spacings (figure 11).

To calculate dose in an homogenous medium, TERMA is convolved with the kernel $D = T \cdot K$.

To create a beam model that agrees with measured data, there are a number of parameters to play with, including the following:

- Spectrum: on axis and off axis.

- Primary beam profile: derived from in-air or from shallow profile for large field.

- Gaussians sigmas for geometrical penumbra.

- Electron contamination: to get the initial few mm of the PDD correct.

Providing one is doing a true convolution (i.e. with a spatially invariant kernel), one can make calculations much faster by the use of Fast Fourier

$$FFT(f \otimes g) = FFT(f) \times FFT(g)$$

Transform (FFT) methods:

$$f \otimes g = FFT^{-1}(FFT(f) \times FFT(g))$$

Hence:

Multiplying is much faster than convolving. A 1D convolution of two arrays of length N will require N^2 calculations. In 3D, this becomes N^6 . FFT is of the order of $N \log_2(N)$ in 1D, and $N^3 \log_2(N)$ in 3D.

For example, for $N = 256$, $N^6 = 2.8 \times 10^{14}$ and $N^3 \log_2(N) = 1.3 \times 10^8$ (a million times less).

It will be seen from these equations that FFT convolution requires an invariant kernel. In other words, the width of the kernels used to blur the dose distribution does not vary with position. This approximation is fine in a water tank. However, in a patient the width of the kernel will increase as density decreases, and vice versa. This means that algorithms that rely on FFT convolutions cannot model the variation of penumbra with density.

Superposition

In a 'type b' algorithm, the shape of the kernel depends on the densities between the interaction point and the dose calculation point. Therefore, we no longer have a true convolution so it cannot be computed in Fourier space. Even in a water tank, the kernel is not truly invariant as the kernels should really be 'tilted' to follow the divergence of the beam; this issue can lead to differences at the edge of large fields. If one is performing an operation similar to convolution, but with a kernel that varies with position, one is no longer performing a convolution; one is instead performing a superposition. This has a major impact on calculation speeds.

FFT is much faster than brute force convolution, but only works for an invariant kernel. This is part of the reason why 'type a' algorithms are faster than 'type b' algorithms.

Collapsed cone algorithm

The solution to this dilemma, which is used by a number of planning systems, is the collapsed cone algorithm. This is illustrated in figure 12.

- Divide the space around a point into a series of cones.
- Assume that all energy released in the cone is transported and deposited along the axis.
- Calculation time is of the order of MN^3 where M is the number of cones considered at each point.

When commissioning a planning system that uses collapsed cone, there are several questions you should ask. How many rays do they use? (More rays means more accurate but slower.) Do they tilt the kernel? (Not all of them do.) How are they modelling the TERMA? The answers to the questions will help you understand the strengths and weaknesses of the implementation, and make testing the system easier.

Pencil kernel models

If a convolution is done in 2D, as shown in figure 7, the 2D kernel can be referred to as a 'pencil kernel', which is a 2D version of the point kernel described above. The kernel varies with depth, but is usually invariant within a plane. This makes it a 'type a' algorithm and it can be calculated using FFT convolution, giving the so-called 'pencil beam models'. It is also possible to have pencil kernels scaled within a plane, giving a 'type b' algorithm.

Anisotropic analytical algorithm (AAA)

This algorithm is 'anisotropic', i.e. it is a 'type b' algorithm, and 'analytical' – it uses an analytical method, not FFT. Essentially, it is a combination of a triple Gaussian pencil beam model with a 1D depth scatter kernel model. Lateral density scaling is applied to the pencil beams. The 1D depth scatter kernel is scaled for local density. It utilises a multisource model: primary, extra-focal, electron contamination and wedge.

The pencil beam is modelled as a superposition of Gaussian sources. The convolution of a Gaussian with a step function is an error function (see the section on convolution above), so the algorithm analytically superimposes lots of scaled error functions.

Solution of the linear Boltzmann transport equation

The most recent class of 'type b' algorithms to make it into a commercial system are based on solutions of the linear Boltzmann transport equation (LBTE). This method is the basis of the Accuros algorithm in Eclipse. The Boltzmann transport equation (BTE) describes the behaviour of photons and particles as they pass through and interact with matter. The non-linear form of the equation can model interactions between charged particles (e.g. Coulomb repulsion of electrons) whilst the linear form assumes that particles only interact with the matter they are passing through. The implementation in Accuros solves a time-independent three-dimensional system of coupled Boltzmann transport equations with the aim of modelling the distribution of angular photon and electron fluence within a patient. The equations include terms which describe photon and electron scattering, production and attenuation (specifically, electron attenuation based on stopping powers).

Unlike Monte Carlo, which uses random numbers to follow histories, Accuros uses numerical methods to explicitly solve the LBTE. In principal, both Monte Carlo and LBTE methods would converge to the same answer if all computational approximations were removed (and enough time allowed for calculation), since they would both be limited by the same uncertainties inherent in the cross-section data. In practice, both methods use approximations to speed up calculations, so neither is exact. LBTE is more prone to systematic errors from the fact that a continuously variable function is cut up into discrete steps of position, energy and angle, whilst Monte Carlo is more prone to random errors from insufficient numbers of histories being used, and also suffers from some discretisation errors. The implementation in Eclipse uses the same multiple source model as AAA to simplify the configuration process for users that have already implemented AAA.

One interesting feature of the LBTE algorithm is that the calculation time is virtually independent of the number of beams being calculated. This means that it will appear slow when used to calculate a single beam, but fast when

being used to calculate a complex VMAT plan.

Measured beam models

When measuring beam data to enter into a planning system, a large proportion of the data is measured on the central axis. Readers who wish to have a good understanding of central axis dose calculation should read the appendices of *BJR* supplement 25.⁸ The required data include the following:

- Output factors with and without phantom scatter (any two out of S_c, S_p, S_{pc}).
- Some sort of depth dose data (PDD, TMR, TPR, TAR, etc).
- Data on absorbers (wedges, trays, etc.).

The extent to which your planning system will use this data depends on the dose calculation models used:

- Measured beam data systems will use the data in the calculation; the algorithms will interpolate into output and depth dose data by equivalent square and depth. Whilst measured beam models have been superseded in commercial planning systems, they are still in use in some check systems, (commercial and in-house) because they are relatively simple to implement.
- Pencil beam models use nearly all of the data. Central axis data will be used directly, whilst profile data will be used to check the models.
- Convolution/superposition models will use some of the data to check the models, and some of it (especially the output data) to normalise predictions back to reality at a number of field sizes.
- Monte Carlo models shouldn't need to use the data (other than to normalise the dose per MU for the reference field size), but you will want to use them to check your results.

Measured beam data is usually measured in water tanks.

Whilst the dose on the central axis can be characterised with relatively few measurements, with simple means of interpolating between measurements, the beam profiles (dose off-axis) are more complex. Figure 13 shows the problem.

The problem of how to interpolate between depths was solved in 1974 by Milan and Bentley,⁹ who normalised each curve on the central axis and

→ PART 2

of this tutorial, in the next issue of Scope, will cover density corrections, inverse planning and optimisation algorithms, the effects on planning of magnetic fields, and dose calculations for particle therapy

→ CONTACT

If you have a comment on this article please email Simon Thomas:

simon.thomas@addenbrook.es.nhs.uk

plotted each curve as a function of angle from the central axis. Figure 14 illustrates this. It is now straightforward to interpolate between depths.

The algorithm originally specified measuring on 47 fan lines at five depths. This was designed to keep the memory requirements low, in the days when computers had only a few kB of memory. Since this is no longer a limitation, modern implementations of this algorithm can use more depths and points, limited only by your willingness to measure the data in a plotting tank.

If you test your planning system by looking at how well it reproduces the measured data, these

models will appear to be excellent. However for irregular fields, especially those defined with MLC, and for situations with loss of scatter such as tangential fields, these algorithms show severe limitations.

→ ACKNOWLEDGEMENTS

I am grateful to my colleagues Chris Rose, Harpreet Dhiraj and Stacey Holloway for comments on versions of this tutorial.

I am grateful to the vendors for sending me details of how their algorithms have been implemented.

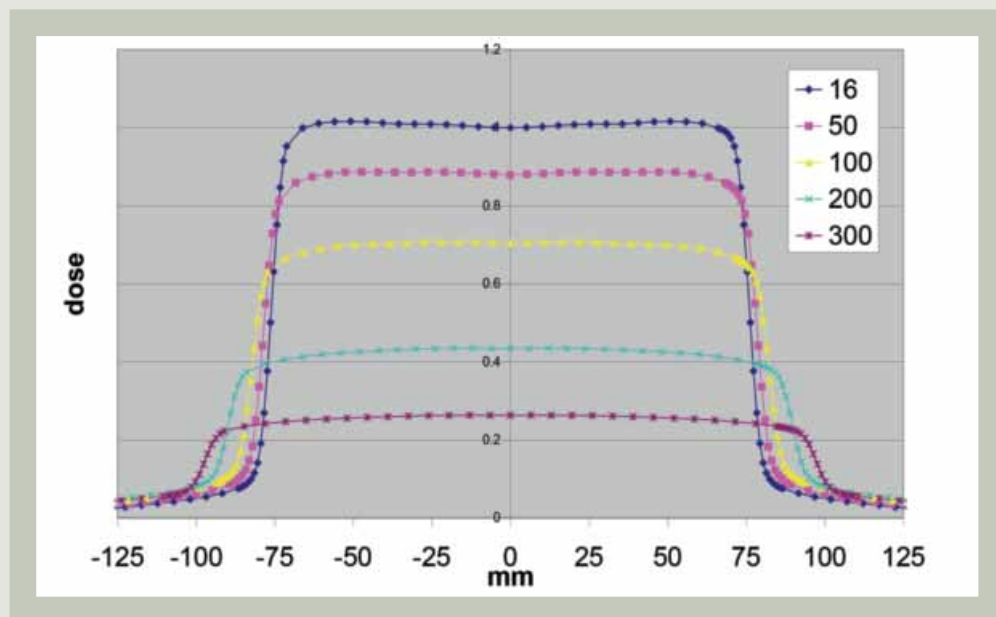


FIGURE 13. Beam profiles for a 15 cm-wide beam of 6 MV x-rays, at 100 cm SSD, shown at depths from 16–300 mm

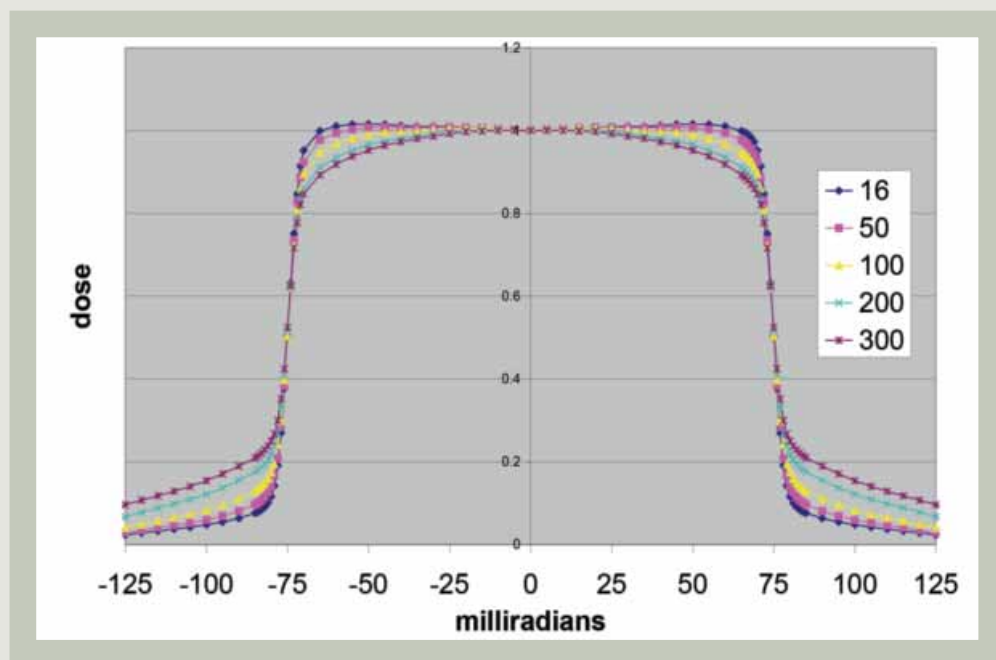


FIGURE 14. The data of figure 13, where the distance in mm has been replaced by angle from central axis in milli-radians

REFERENCES

- 1 **Knöös T, Wieslander E, Cozzi L et al.** Comparison of dose calculation algorithms for treatment planning in external photon beam therapy for clinical situations. *Phys Med Biol* 2006; 51(22): 5785–807.
- 2 **Kawrakow I, Fippel M, Friedrich K.** 3D electron dose calculation using a Voxel based Monte Carlo algorithm (VMC). *Med Phys* 1996; 23(4): 445.
- 3 **Fippel M.** Fast Monte Carlo dose calculation for photon beams based on the VMC electron algorithm. *Med Phys* 1999; 26(8): 1466.
- 4 **Neuenschwander H, Born EJ.** A macro Monte Carlo method for electron beam dose calculations. *Phys Med Biol* 1992; 37(1): 107–25.
- 5 **Kawrakow I, Rogers D.** *The EGSnrc Code System: Monte Carlo Simulation of Electron and Photon Transport.* Ottawa: National Research Council of Canada, 2000.
- 6 **Andreo P.** Dose to ‘water-like’ media or dose to tissue in MV photons radiotherapy treatment planning: still a matter of debate. *Phys Med Biol* 2015; 60(1): 309–37.
- 7 **Ahnesjö A.** Collapsed cone convolution of radiant energy for photon dose calculation in heterogeneous media. *Med Phys* 1989; 16(4): 577.
- 8 **British Journal of Radiology.** Central axis depth dose data for use in radiotherapy. *Brit J Radiol* 1996: supplement 25.
- 9 **Milan J, Bentley RE.** The storage and manipulation of radiation dose data in a small digital computer. *Brit J Radiol* 1974; 47(554): 115–21.